

ResNet-50 with Class Reweighting and Anatomy-Guided Temporal Decoding for Gastrointestinal Video Analysis

Romil Intiaz^a, Dimitris K. Iakovidis^a

^a Department of Computer Science and Biomedical Informatics, University of Thessaly, Papasiopoulou 2–4, Lamia 35131, Greece

Corresponding Author Email: rimitiaz@uth.gr

Team Name: EndoInsight

GitHub Repository Link: <https://github.com/romilintiaz/ResNet-50-for-GI-Events>

Abstract

We developed a multi-label gastrointestinal video analysis pipeline based on a ResNet-50 frame classifier followed by anatomy-guided temporal event decoding. The system predicts 17 labels, including 5 anatomy classes and 12 pathology classes, from frames resized to 336×336 . A major challenge was severe class imbalance, particularly for rare pathology labels. To address this, we used clipped class-wise positive weighting in the training loss, which improved rare-class learning while maintaining stable optimization. At the temporal stage, we found that direct frame-to-event conversion produced fragmented mismatches with the official ground truth. The final submission therefore combined GT-style framewise event composition, anatomy vote smoothing, and anatomy-based pathology gating with a conservative hysteresis decoder. This design improved the final temporal mAP from 0.3801 to 0.4303 on the challenge test set.

1 Motivation

Automatic understanding of gastrointestinal video is important for computer-assisted diagnosis, lesion screening, and efficient review of long clinical examinations. However, rare abnormal findings are difficult to detect reliably because they may appear only briefly, coexist with changing anatomy, and be represented by very few training samples. We participated in this challenge to study how far a robust frame-level visual model can be pushed toward temporally consistent event detection under a strict sequential evaluation setting. In particular, the challenge is important because it requires not only correct recognition of individual frames, but also correct localization of event boundaries over time.

2 Methods

Our pipeline consisted of a frame-level classifier followed by temporal event construction. Among the tested backbones, ResNet-50 [1] provided the best balance between stability, speed,

and predictive performance, and was therefore selected as the core model. Each frame was resized to 336×336 and processed independently to predict the presence of 17 labels. The label space contained 5 anatomy classes (mouth, esophagus, stomach, small intestine, and colon) and 12 pathology classes.

Let x_i denote the i -th frame and $y_{ic} \in \{0, 1\}$ the ground-truth label for class c . For each class, the network outputs a real-valued score z_{ic} before probability normalization. This score is transformed into a probability using the sigmoid function:

$$p_{ic} = \sigma(z_{ic}) = \frac{1}{1 + e^{-z_{ic}}}, \quad (1)$$

where p_{ic} represents the predicted probability that class c is present in frame i .

At the frame level, the model was trained using weighted binary cross-entropy [2]. For class c , the loss was defined as

$$\mathcal{L}_c = -\frac{1}{N} \sum_{i=1}^N [w_c y_{ic} \log(p_{ic}) + (1 - y_{ic}) \log(1 - p_{ic})], \quad (2)$$

where N is the number of training frames and w_c is the positive class weight for class c . The total loss over all classes was

$$\mathcal{L} = \sum_{c=1}^C \mathcal{L}_c, \quad C = 17. \quad (3)$$

2.1 How was class imbalance handled?

Class imbalance was one of the main challenges in this work. The dataset contained many more frames for common anatomy classes, whereas several pathology classes had only a small number of positive samples. Without weighting, the model quickly became biased toward frequent classes, and rare labels showed very weak learning signals.

To address this, we computed a positive class weight for each class c based on the ratio of negative to positive samples:

$$w_c = \frac{N_{\text{neg},c}}{N_{\text{pos},c}}, \quad (4)$$

where $N_{\text{pos},c}$ and $N_{\text{neg},c}$ denote the numbers of positive and negative training samples for class c , respectively. This increased the penalty for mistakes on rare classes and encouraged the model to learn minority categories more effectively.

Because some classes were extremely rare, the raw weights could become excessively large and destabilize optimization. Therefore, we clipped the weights into a safe interval:

$$w_c = \min(\max(w_c, w_{\min}), w_{\max}), \quad (5)$$

where $w_{\min} = 1.0$ and $w_{\max} = 50.0$ in our experiments. This clipping prevented exploding gradients and reduced training instability.

We also explored focal-loss-style weighting [3], written in our setting as

$$\mathcal{L}_{\text{focal}} = -\frac{1}{N} \sum_{i=1}^N \sum_{c=1}^C (1 - p_{ic})^\gamma [w_c y_{ic} \log(p_{ic}) + (1 - y_{ic}) \log(1 - p_{ic})]. \quad (6)$$

However, while focal loss sometimes improved rare-class sensitivity, it was not consistently stable for extremely low-frequency labels. In practice, the clipped class-weighting strategy was one of the most important components of the pipeline. Without weighting, rare pathology classes showed near-zero recall; with weighting, rare-class gradients increased and recall improved; and with clipped weighting, this improvement was achieved without causing unstable optimization.

2.2 Temporal decoding and event construction

At the temporal level, frame probabilities were converted into event predictions. A baseline hysteresis-style decoder was first used to map framewise scores into temporal segments. However, temporal debugging on the training set revealed a major mismatch between predictions and the official event-level ground truth: the ground truth was fragmented whenever the full active label set changed, whereas our initial predictions were fewer and longer. To analyze this systematically, we built a dedicated debugging pipeline that generated temporal JSON files for both ground truth and predictions and reported per-video and per-label segment counts.

To reduce this mismatch, we first composed final events from framewise active labels in the same style as the official ground truth. Specifically, if the active label set at frame t is denoted by \mathcal{S}_t , then a new temporal event is started whenever $\mathcal{S}_t \neq \mathcal{S}_{t-1}$.

2.3 Anatomy vote smoothing

We further stabilized anatomy predictions using a local voting window. For a frame t , we considered a neighborhood

$$\mathcal{W}_t = \{t - r, \dots, t, \dots, t + r\}, \quad (7)$$

where r is the window radius. Let \hat{a}_τ be the predicted anatomy class at frame τ . The final anatomy label at frame t was obtained by majority voting:

$$a_t = \arg \max_k \sum_{\tau \in \mathcal{W}_t} \mathbf{1}[\hat{a}_\tau = k]. \quad (8)$$

In our final setting, a window size of 1 was selected, which effectively avoided over-smoothing while still preserving true anatomical transitions.

2.4 Anatomy-based pathology gating

We also introduced an anatomy-guided gating mechanism for pathology predictions. The idea is that some abnormalities are anatomically plausible only in specific regions. Let $p_t^{(m)}$ denote the pathology probability for class m at frame t , and let \mathcal{A}_m denote the set of anatomies where

pathology m is allowed according to our anatomy-gating prior. The gated pathology probability was defined as

$$\tilde{p}_t^{(m)} = \begin{cases} p_t^{(m)}, & \text{if } a_t \in \mathcal{A}_m, \\ 0, & \text{otherwise.} \end{cases} \quad (9)$$

This step suppressed anatomically implausible pathology predictions and reduced false positives in regions where the target abnormality should not occur.

2.5 Final temporal decoder

After anatomy vote smoothing and pathology gating, the final pathology sequence was decoded using the default hysteresis-based temporal decoder. Compared with more aggressive support-window decoding, the conservative decoder generalized better on unseen data and gave the best final test result. We also tested an HMM/Viterbi-based decoder [4] with temperature scaling [5], but the final chosen system remained the simpler and more stable anatomy-guided hysteresis pipeline.

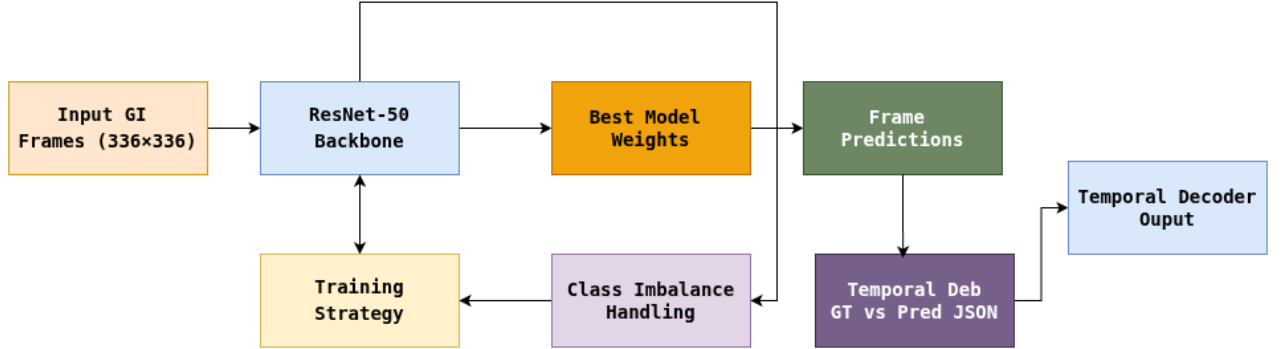


Figure 1: Overall flowchart of the proposed ResNet-50-based temporal event detection pipeline.

Figure 1 illustrates the overall workflow of the proposed method. First, gastrointestinal video frames are resized to 336×336 and passed through a ResNet-50 backbone for frame-level prediction. During training, the model is optimized using a dedicated training strategy together with class-imbalance handling, which is one of the key components of the pipeline. The best-performing model weights are then used to generate frame-level predictions. To better understand the gap between frame-level and temporal performance, a temporal debugging stage is introduced by comparing ground-truth and predicted JSON events. Finally, a temporal decoder converts the frame-level outputs into sequential event predictions in the official challenge format.

3 Results

At the frame level, the ResNet-50 backbone achieved a strong performance of approximately **0.8605 mAP** in 5-fold evaluation, confirming that the model learned discriminative visual

features for both anatomy and pathology classes.

Our initial baseline temporal pipeline achieved an overall temporal mAP of **0.3801**. After introducing anatomy vote smoothing, anatomy-based pathology gating, and GT-style framewise event composition while keeping the default hysteresis decoder, the final temporal performance improved to:

- **Overall mAP @ 0.5 = 0.4303**
- **Overall mAP @ 0.95 = 0.4020**

This corresponds to a net improvement of **+0.0502 mAP** over the temporal baseline.

For the final challenge-style temporal evaluation on the three test videos, the obtained per-video results were:

- **ukdd_navi_00051: mAP@0.5 = 0.5319, mAP@0.95 = 0.5000**
- **ukdd_navi_00068: mAP@0.5 = 0.3533, mAP@0.95 = 0.3529**
- **ukdd_navi_00076: mAP@0.5 = 0.4056, mAP@0.95 = 0.3529**

A summary of the temporal results is given in Table 1.

Table 1: Summary of temporal results.

Evaluation	mAP@0.5	mAP@0.95
Baseline temporal pipeline	0.3801	–
Training temporal analysis	0.7236	0.6780
Test video ukdd_navi_00051	0.5319	0.5000
Test video ukdd_navi_00068	0.3533	0.3529
Test video ukdd_navi_00076	0.4056	0.3529
Final overall test temporal	0.4303	0.4020

These results show that frame-level recognition was substantially stronger than event-level localization, but also confirm that anatomically informed temporal refinement improved performance. In particular, anatomy-based pathology gating reduced anatomically implausible false positives, while the local anatomy voting strategy stabilized region labels without blurring true transitions.

4 Discussion

The main lesson from this challenge was that strong frame-level classification does not directly translate into strong temporal event detection. Our debugging experiments showed that the official ground truth was highly fragmented according to the full active label set, whereas early predictions were smoother and contained fewer segments. This mismatch significantly reduced temporal IoU matching even when the frame-level predictions were visually reasonable.

We also observed that more aggressive temporal decoders could improve training-set temporal mAP, but these gains did not consistently transfer to unseen videos. In contrast, the combination of GT-style event composition, anatomy vote smoothing, and anatomy-based pathology gating improved the final test performance while preserving stable decoding behavior. The most robust final system was therefore a stable frame classifier combined with anatomically informed temporal refinement rather than a highly aggressive temporal model.

Future improvements could include end-to-end temporal training, sequence-aware architectures, or more advanced anatomical priors. However, within the available time budget, the most effective strategy was to combine a strong frame classifier with carefully designed temporal event construction.

5 Summary

Team **EndoInsight** utilized **ResNet-50** [1] as the main AI model. A key component of the proposed pipeline was the use of **clipped class-wise positive weighting** to address severe class imbalance, particularly for rare pathology classes. In the temporal stage, **anatomy vote smoothing**, **anatomy-based pathology gating**, and **GT-style framewise event composition** improved the consistency of event prediction and reduced anatomically implausible detections. The team improved the baseline temporal mAP from **0.3801** to a final overall **mAP@0.5 of 0.4303**, with an overall **mAP@0.95 of 0.4020**.

6 Acknowledgments

This work has been funded by the European Union Marie Curie Skłodowska Action (MSCA), grant agreement No. 101169012, project Intelli-Ingest (<https://www.intelli-ingest.com/>).

As participants in the ICPR 2026 RARE-VISION Competition, we fully comply with the competition’s rules as outlined in [6]. Our AI model development is based exclusively on the datasets in the competition. The mAP values are reported using the test dataset and sanity checker released in the competition.

References

- [1] Kaiming He, Xiangyu Zhang, Shaoqing Ren, and Jian Sun. Deep residual learning for image recognition. In *Proceedings of the IEEE Conference on Computer Vision and Pattern Recognition*, pages 770–778, 2016.
- [2] Ian Goodfellow, Yoshua Bengio, and Aaron Courville. *Deep Learning*. MIT Press, 2016. URL <https://www.deeplearningbook.org/>.
- [3] Tsung-Yi Lin, Priya Goyal, Ross Girshick, Kaiming He, and Piotr Dollár. Focal loss for dense object detection. In *Proceedings of the IEEE International Conference on Computer Vision*, pages 2980–2988, 2017.

- [4] Lawrence R. Rabiner. A tutorial on hidden markov models and selected applications in speech recognition. *Proceedings of the IEEE*, 77(2):257–286, 1989.
- [5] Chuan Guo, Geoff Pleiss, Yu Sun, and Kilian Q. Weinberger. On calibration of modern neural networks. In *Proceedings of the 34th International Conference on Machine Learning*, volume 70, pages 1321–1330, 2017.
- [6] Anni Lawniczak, Manas Dhir, Maxime Le Floch, Palak Handa, and Anastasios Koulaouzidis. ICPR 2026 RARE-VISION Competition Document and Flyer. 12 2025. doi: 10.6084/m9.figshare.30884858.v3. URL https://figshare.com/articles/preprint/ICPR_2026_RARE-VISION_Competition_Document_and_Flyer/30884858.